Article:
Camacho Corzo, DM, Borissova, A, Hammond, RB et al. (2014) Nucleation mechanism and kinetics from the analysis of polythermal crystallisation data: Methyl stearate from kerosene solutions. CrystEngComm, 16 (6). pp. 974-991. ISSN: 1466-8033

https://doi.org/10.1039/c3ce41098f

DETERMINATION OF THE NUCLEATION MECHANISM AND KINETICS FROM THE ANALYSIS OF POLYTHERMAL CRYSTALLISATION DATA: METHYL STEARATE FROM KEROSENE SOLUTIONS

Diana M. Camacho Corzo[a], Antonia Borissova[a], Robert B. Hammond[a] , Dimo Kashchiev[b], Kevin J. Roberts[a*], Ken Lewtas[c], Iain More[c]

[a] Institute of Particle Science and Engineering and Institute of Process Research and Development, School of Process, Environment and Materials Engineering, University of Leeds, Leeds, LS2 9JT, UK

[b] Institute of Physical Chemistry, Bulgarian Academy of Sciences, ul. Acad. G. Bonchev 11, Sofia 1113, Bulgaria

[c] Infineum UK Ltd, Milton Hill Business and Technology Centre, Abingdon, OX13 6BB, UK

Keywords: Solution Crystallisation, Polythermal and Isothermal Methods, Critical Undercooling, Relative Critical Undercooling, Nucleation, Instantaneous Nucleation, Progressive Nucleation, Biodiesel Fuels, Fatty Acid Methyl esters.

*Corresponding author

Submitted to the CrystEngComm, revised manuscript 01th September 2013

ABSTRACT

A polythermal methodology to assess the mechanisms and the kinetics of solution crystallisation is described and used in connection with a recently proposed model for the dependence of the critical undercooling for crystallisation on the cooling rate (D. Kashchiev, A. Borissova, R. B. Hammond, K. J. Roberts, J Cryst Growth, 312 (2010) 698–704; J Phys Chem B, 114 (2010) 5441–5446). This first principles model allows determination of crystallisation parameters that could otherwise only be obtained by combined application of both the isothermal and the polythemal methods. The methodology is validated through analysis of experimental data measured for methyl stearate crystallising from kerosene solutions with concentrations from 200 to 350 g/l. The analysis reveals a progressive heterogeneous nucleation mechanism and crystallite interfacial tension values between 1.64 and 1.79 $\frac{mJ}{m^2}$ with no obvious dependence on the solution concentration, in good agreement with values derived by isothermal methods. Sensitivity analysis leads to the conclusion that a minimum of four different cooling rates spanning at least one order of magnitude together with at least five repeats for crystallisation temperature values at each cooling rate are appropriate. Extensive supplementary material provides a mathematical description of the above authors' model, insight into the relationship between this model and the empirical Nyvlt model, and further detail concerning the results of the sensitivity analysis carried out on the experimental methodology used.

1. INTRODUCTION

Crystallisation in solutions has been the subject of numerous studies due to its importance in many industrial processes and applications. In particular, the problem of the effect that the cooling rate has on the metastable zone width ($MSZW$) has recently been dealt with in a comprehensive theoretical study [1, 2]. A detailed understanding of crystallisation phenomena is not only required to help design chemical separation and purification processes, but also to prevent the appearance of crystals when they are not desired. As an example, crystallisation in biodiesel fuels can impact negatively on their cold flow properties representing a potential problem for their use in practical fuel formulations [3].

In general, some solutes tend to crystallise when the solution homogeneous-phase is subject to a change in its conditions. In crystallisation, however, the crystal characteristics are determined not only by the chemical and phase composition, but also by the kinetics of the process. The supersaturation is the driving force of crystallisation. A supersaturated solution can remain metastable until a critical level of supersaturation corresponding to the $MSZW$, is reached. The $MSZW$ defines the kinetic limit of metastability and provides a useful indication of the ease with which crystallisation will occur. Thus, it is an important parameter in the analysis of crystallisation processes as it can be considered a crystallisation property for each system [4].

The $MSZW$ is essentially the solution critical undercooling for crystallisation,(ΔT_c), expressed as the difference between the system saturation (or equilibrium) temperature (T_e) and the temperature (T_c) at which a detectable crystallisation commences: $\Delta T_c = T_e - T_c$. The onset of crystallisation however is not unique, as it will greatly depend on a number of

crystallisation environmental parameters all of which could have an influence on the crystal nucleation and growth kinetics [5].

Isothermal and polythermal crystallisation methodologies both use the concept of metastability to study crystallisation processes. The former usually makes use of expressions derived from classical nucleation theory to relate the induction time (τ) to the supersaturation ratio (S) in order to determine the nucleus interfacial tension and the nucleus size . To obtain crystallisation parameters, the polythermal methodology generally utilises expressions that predict the effect of the solution cooling rate q on the critical undercooling ΔT_c. Until recently, the interpretation of polythermal $\Delta T_c(q)$ data has been based on an essentially empirical methodology. In particular, researchers have mostly used Nyvlt's expression, derived from an empirical formula for the nucleation rate, which predicts a linear increase in $ln\,\Delta T_c$ with $ln\,q$ [6, 7]. However, whilst this relationship is most useful in terms of crystallisation process characterisation, this empirical approach has not contributed significantly to developing a mechanistic understanding of crystallisation processes. Later, Kubota [8] used the concept that for a given system, the extent of the measured $MSZW$ depends on the sensitivity of the method of detection employed to observe the first appearance of nuclei. He proposed a theoretical model, predicting also linearity between $ln\,\Delta T_c$ and $ln\,q$, which starts from the assumption that the measured $MSZW$ corresponds to the undercooling at which the number density of accumulated grown primary nuclei has reached a fixed (but unknown) value. Recently, employing the classical nucleation theory, Sangwal [5, 9, 10] obtained a $\Delta T_c(q)$ formula which provides physical insight into the parameters associated with it and which reveals linearity between $\frac{1}{(\Delta T_c)^2}$ and $\ln q$. More recently Kashchiev, Borissova, Hammond and Roberts ($KBHR$) developed an analytical approach [1, 2], based on that of Kolmogorov-Johnson-Mehl-Avrami ($KJMA$), which led to

$\Delta T_c(q)$ expressions derived from the initial temporal evolution of either the fraction (α) of crystallised volume or the number (N) of nucleated crystallites. The expressions derived, when applied to experimental data, not only allow the determination of key parameters associated with both the nucleation and the growth processes, but also make it possible to gain an insight into the nucleation mechanism by differentiating between instantaneous nucleation (IN) and progressive nucleation (PN).

This paper applies the $KBHR$ [1, 2] approach to characterise the nucleation kinetics of methyl stearate crystallising from kerosene solutions. In this, a large set of experimental $T_c\ (q)$ data was collected and analysed with the aim of validating an experimental procedure for the application of this approach to crystallisation systems of practical interest.

2. THEORY

2.1 Nucleation processes

The characterisation of crystallisation processes can not only be undertaken from a thermodynamic point of view, but also requires analysis of the process kinetics. Crystallisation not only depends on reactant concentrations or reaction order but is usually affected by several additional factors such as the solute diffusion and crystal geometrical shape [11]. As a result, other parameters such as the crystal interfacial tension (γ) and $MSZW$ also become important.

Crystallisation can take place either by a mononuclear or polynuclear nucleation mechanism [11]. The polynuclear mechanism occurs under conditions that favour the formation of statistically many nuclei and is often expressed in two different ways known as instantaneous nucleation IN and progressive nucleation PN. Whilst in PN new crystal nuclei are continuously formed in the presence of the already growing ones [1, 11], in the case of IN all nuclei emerge at once at the beginning of the crystallisation process to subsequently grow and develop into crystals [2, 11].

As in the case of IN all nuclei are formed simultaneously, at any time, the solution will contain a fixed number of crystallites of the same size, assuming they all grow at the same rate [2, 11]. This kinetic pathway is often followed by heterogeneous nucleation (HEN) which is favoured when strongly nucleation active sites are provided, e.g., when impurity molecules and foreign particles are present in the solution.

In the case of PN, the nuclei are formed during an extended period of time. Crystal nucleation and growth then occur simultaneously and the solution contains crystals of various sizes at any given point in time [1, 11]. Homogeneous nucleation (HON) as well as secondary nucleation and HEN on relatively weak nucleation-active sites can manifest themselves by means of this type of transformation. A simple scheme summarizing this classification is presented below.

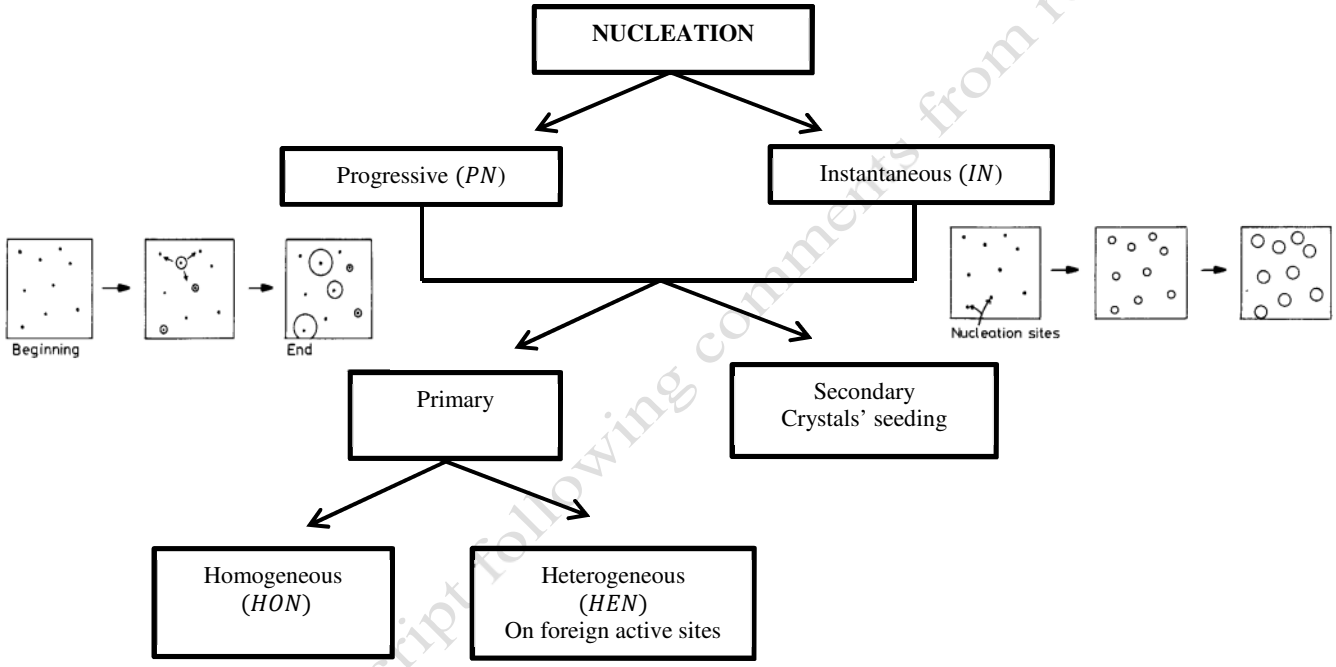

Fig. 1 Schematic diagram highlighting the classification of the various mechanisms important in nucleation processes

Regardless of the mechanism by which the crystals are formed , the solution appears to remain unaffected until the level of supersaturation corresponding to the $MSZW$ is reached [12]. The $MSZW$ depends on the crystallites nucleation and growth kinetics, which in turn are influenced by a number of crystallisation environmental parameters such as the equilibrium (or saturation) temperature T_e, cooling rate q, solution agitation, presence of impurities and seeds and the solvents used [1, 12]. Alternative expressions for the $MSZW$ can be given in terms of either concentration or temperature. Among the most common are those for the

maximum concentration difference (ΔC_{max}) and the critical undercooling ΔT_c. The former quantity is defined as:

$$\Delta C_{max} = C_{max} - C_e \quad (1)$$

where C_{max} is the solution concentration at the limit of metastability, and C_e is the equilibrium solution concentration (or the solubility).

Similarly, the critical undercooling ΔT_c is defined as:

$$\Delta T_c = T_e - T_c \quad (2)$$

where T_e and T_c are the solution equilibrium and crystallisation temperatures, respectively.

A dimensionless quantity associated with the critical undercooling ΔT_c is the relative critical undercooling (u_c) given by:

$$u_c = \frac{\Delta T_c}{T_e} \quad (3)$$

Two broad classes of experimental methods are mainly used to characterise a crystallisation process:

- The polythermal method which is based on determination of the $MSZW$ and the effect exerted on it by the rate at which supersaturation is created.

- The isothermal method which is based on determination of the induction time (τ), i.e. the time taken for crystallisation to be detected at constant temperature and the influence of the supersaturation on this time.

2.2 Polythermal method

In the polythermal method, the critical undercooling ΔT_c is measured as a function of the cooling rate q and the data collected are analysed by means of any of the approaches previously developed for the $\Delta T_c(q)$ dependence. In the case of the Nyvlt approach [6, 7],the logarithms of q and ΔT_c are predicted to be linearly related. This $\Delta T_c(q)$ dependence was derived by assuming that the decrease in supersaturation is solely due to the depletion of solute by the nucleating crystallites. The effect of the subsequent growth of these crystallites on this decrease was not accounted for because Nyvlt's approach was developed for modelling the early stage of the crystallisation process, where the limit of metastability corresponds to the moment at which the first crystals are formed, where their surface areas can be considered to be negligibly small. At such a moment the solution concentration would hardly surpass the limit of metastability as a great amount of crystals would be formed leading to a rapid drop in supersaturation.[6, 9, 13-16]. In this particular case, through a material balance, the rate $\left(\frac{dC_e}{dT}\right)q$ of supersaturation change by cooling can be correlated to the nucleation rate as expressed through the following semi-empirical formula:

$$J = k_j(\Delta C_{max})^{m_0} = \frac{dC_e}{dT}q \tag{4}$$

where J is the nucleation rate, $k_j$is an empirical parameter , m_0 is the order of nucleation, $\Delta C_{max} = \frac{dC_e}{dT}\Delta T_c$ and $\frac{dC_e}{dT}q$ represents the number of solute molecules precipitated per unit time and unit volume.

According to equation (4) $ln\,\Delta T_c$ depends linearly on $ln\,q$ and hence analysis of experimental $\Delta T_c(q)$ data in a $ln-ln$ correlation results in the determination of the two empirical parameters k_j and m_0.

Although widely used, the Nyvlt approach has received some criticism mainly due to its semi-empirical nature, as the two nucleation parameters used lack any direct physical significance and also the growth of the generated nuclei to detectable size is neglected [1, 5].

More recently, the $KBHR$ approach [1, 2] has led to alternative expressions that overcome some of the drawbacks of the previous approaches [5, 6, 8-10]. These expressions do not contain empirical parameters and allow PN-rulled crystallisation to be distinguished from that mediated by IN, because while, in the former case the critical undercooling ΔT_c depends on both the nucleation and the growth rate of the crystallites, in the latter case, it is only controlled by the growth rate of the instantaneously nucleated crystallites provided their concentration C_o is independently known.

2.2.1 The $KBHR$ Approach

According to the $KBHR$ approach, the dependence of $ln\,\Delta T_c$ on $ln\,q$ is not linear and manifests itself differently depending on the nucleation mechanism involved. This approach applies to the early stage of crystallisation because of its treating the crystallites as not

contacting each other. It makes use of the nucleation rate formula of the classical three dimensional $(3D)$ nucleation theory for stationary HON and HEN. As in practice the limit of metastability can only be registered when crystallites have already grown to a detectable size and/or number, the model presents expressions that relate this limit to either the fraction (α_{det}) of crystallised volume or the number (N_{det}) of nucleated crystallites at the detection point in which both the nucleation and the growth rates of the crystallites would have an influence.

The $KBHR$ approach is based on the $KJMA$ equation [11] for the time dependence of the fraction α of crystallised volume. This fraction is defined as:

$$\alpha = \frac{V_c}{V} \tag{5}$$

where V_c and V are the total crystallite volume and the solution volume respectively

2.2.1.1 Progressive nucleation case

The analytical performing of the integral in the $KJMA$ equation [1, 17] allows obtaining the dependence of the relative critical undercooling u_c on the cooling rate q at the early stage of the crystallisation when u_c meets the inequalities [1]:

$$u_c < 0.1, a u_c < 1 \tag{6}$$

$$u_c < \left(\frac{2b}{3}\right)^{1/2} \tag{7}$$

Here, the dimensionless, molecular latent heat of crystallisation a, is defined by:

$$a = \frac{\lambda}{kT_e} \tag{8}$$

where λ is the molecular latent heat of crystallisation and k is the Boltzmann constant. The dimensionless thermodynamic parameter b of $3D$ nucleation is defined by

$$b = \frac{k_n v_o^2 \gamma_{eff}^3}{kT_e \lambda^2} \tag{9}$$

where k_n is the nucleus shape factor (e.g., $16\pi/3$ for spherical nuclei and 32 for cubic nuclei) [11], v_o is the volume occupied by a solute molecule in the crystal, γ_{eff} is the nucleus effective interfacial tension.

The final expression for the $u_c(q)$ dependence is derived [1] by accounting for the increase of either the number N of crystal nuclei or the crystallised volume fraction α with the steadily increasing undercooling (u) (see also supplementary material). For u_c determined by the number $N_{det}$of crystallites at the detection point this expression is of the form [1]:

$$ln\, q = ln\, q_0 + a_1\, ln\, u_c - \frac{a_2}{(1-u_c){u_c}^2} \tag{10}$$

Here the free parameters a_1, a_2 and q_0 are given by:

$$a_1 = 3 \tag{11}$$

$$a_2 = b \tag{12}$$

$$q_0 = \frac{V K_J T_e}{N_{det}\, 2b} \tag{13}$$

where K_J is the nucleation rate constant.

When equation (10) is derived by means of the fraction α_{det} of crystallised volume at the detection point, the parameters a_1, a_2 and q_0 read [1]:

$$a_1 = 3 + \frac{3nmd}{md+1} \tag{14}$$

$$a_2 = \frac{b}{md+1} \tag{15}$$

$$q_0 = T_e \left\{ \frac{\Gamma[(n+1)md+1] k_v a^{nmd} K_J K_G^{md}}{(n+1)^d\, (2b)^{(n+1)md+1} \alpha_{det}} \right\}^{\frac{1}{(md+1)}} \tag{16}$$

where Γ is the complete gamma function, d is the dimensionality of crystallites growth, i.e. 3 for spheres or cubes, 2 for disks or plates and 1 for needles, k_v is the crystallites growth shape factor, i.e. $\frac{4\pi}{3}$ for spheres, 8 for cubes, πH_0 for disks, $4H_0$ for square plates (H_0 is the

fixed disk or plate thickness), and $2A_0$ for needles (A_0 is the fixed needle cross-sectional area), K_G is the growth rate constant, and n and $m > 0$ are the crystallite growth exponents which are related to the different growth mechanism [18]. The $n = 1$ case corresponds to growth mediated by diffusion of solute towards the crystallite or transfer of solute across the crystal/solution interface. The $n = 2$ case characterises growth controlled by the presence of screw dislocations in the crystallite. The parameter m ranges between ½ and 1: $m = 1/2$ is for growth controlled by undisturbed diffusion of solute, and $m = 1$ is for growth by diffusion of solute through a stagnant layer around the crystallite or for normal or spiral growth limited by transfer of solute across the crystal/solution interface. At $m = 1$ the crystallite radius increases linearly with time [1, 2, 11].

The parameters in the model expression (10) q_0, a_1 and a_2 all have a distinct physical meaning because a_1 relates to the crystallites growth as its value is determined by the growth exponents n, m and d, a_2 is a fraction of or equal to the thermodynamic nucleation parameter b, and q_0 is expressed by parameters of both the nucleation and the growth of the crystallites.

The critical radius of the nucleus (r^*) and the number (i^*) of molecules in the critical nucleus can be calculated from the equations [1]:

$$r^* = \frac{2\gamma_{eff} v_0}{\lambda u} \tag{17}$$

$$i^* = \frac{2bkT_e}{\lambda u^3} \tag{18}$$

2.2.1.2 Instantaneous nucleation case

In the case of IN a similar use of the $KJMA$ equation is possible [2, 17] within the limit established by inequalities (6) but now by taking into account that all crystal nuclei appear simultaneously with a concentration C_o at a moment t_o corresponding to relative undercooling u_0 defined as:

$$u_o = \frac{\Delta T_o}{T_e} \tag{19}$$

Here ΔT_o is given by:

$$\Delta T_0 = T_e - T_0 \tag{20}$$

where T_o is the solution temperature at the time t_o.

Thus the dependence of relative critical undercooling on the cooling rate can be expressed as [2]:

$$\ln q = \ln q_0 + \left(\frac{1}{m}\right) \ln\left[u_c^{(n+1)m} - u_0^{(n+1)m}\right] \tag{21}$$

In this expression $u_0 \geq 0$, $u_c > u_o$ and the parameter q_0 is given by:

$$q_o = \left[\frac{k_v C_o}{(n+1)^d \alpha_{det}}\right]^{\frac{1}{md}} a^n K_G T_e \tag{22}$$

If additionally, the undercooling u_0 at which all nuclei appear simultaneously is small enough to satisfy the inequality:

$$u_o^{(n+1)m} \ll u_c^{(n+1)m} \tag{23}$$

then equation (21) takes the Nyvlt-type form [2]

$$\ln q = \ln q_o + (n+1) \ln u_c \tag{24}$$

As shown by Kashchiev et al. [1], for a small range of q values equation (10) can also be expressed in the form of a Nyvlt-type equation:

$$ln\, q = ln\, Q + \left(3 + \frac{3nmd}{md+1} + \omega a_2\right) ln\, u_c \tag{25}$$

Here the parameter Q is related to q_o and a_2 in equation (10), and ω is a positive number.

Comparing the factor in front of $ln\, u_c$ in equation (24) for the case of IN with the one in equation (25) for the case of PN leads to the important findings of the $KBHR$ approach that this term is always less than three in the IN case and greater than three in the PN case because n, m and ω are positive numbers and typically $n \leq 2$ [2]. This so called "rule of three" [2] is practically very helpful in that when experimental $u_c(q)$ data are plotted in $ln\, q$ vs. $ln\, u_c$ coordinates and fitted by a straight line, the slope of the line will directly indicate the nucleation mechanism, PN or IN, governing the crystallisation process.

Although the application of the presented $KBHR$ expressions for the $u_c(q)$ dependence is restricted by inequalities (6), this restriction is not too severe, as even for rather low values of equilibrium temperature (e.g. $T_e = 273\ K$), the maximum critical undercooling ΔT_c satisfying the first of these inequalities would have a value , large enough from experimental point of view ($27.3\ K$ for the above example). This means that in the above example only when $\Delta T_c >$ 27.3 the model would not be applicable.

A flow chart summary of the procedure needed to practically apply the $KBHR$ approach [1, 2] is given in Fig. 2*.

* A more detailed explanation of the derivation of the expressions here presented is available in the first section of the supplementary material.

Fig. 2 Flowchart describing the procedure to follow in order to apply ($KBHR$) approach for the interpretation of metastable zone width data ($MSZW$) collected by means of the polythermal method

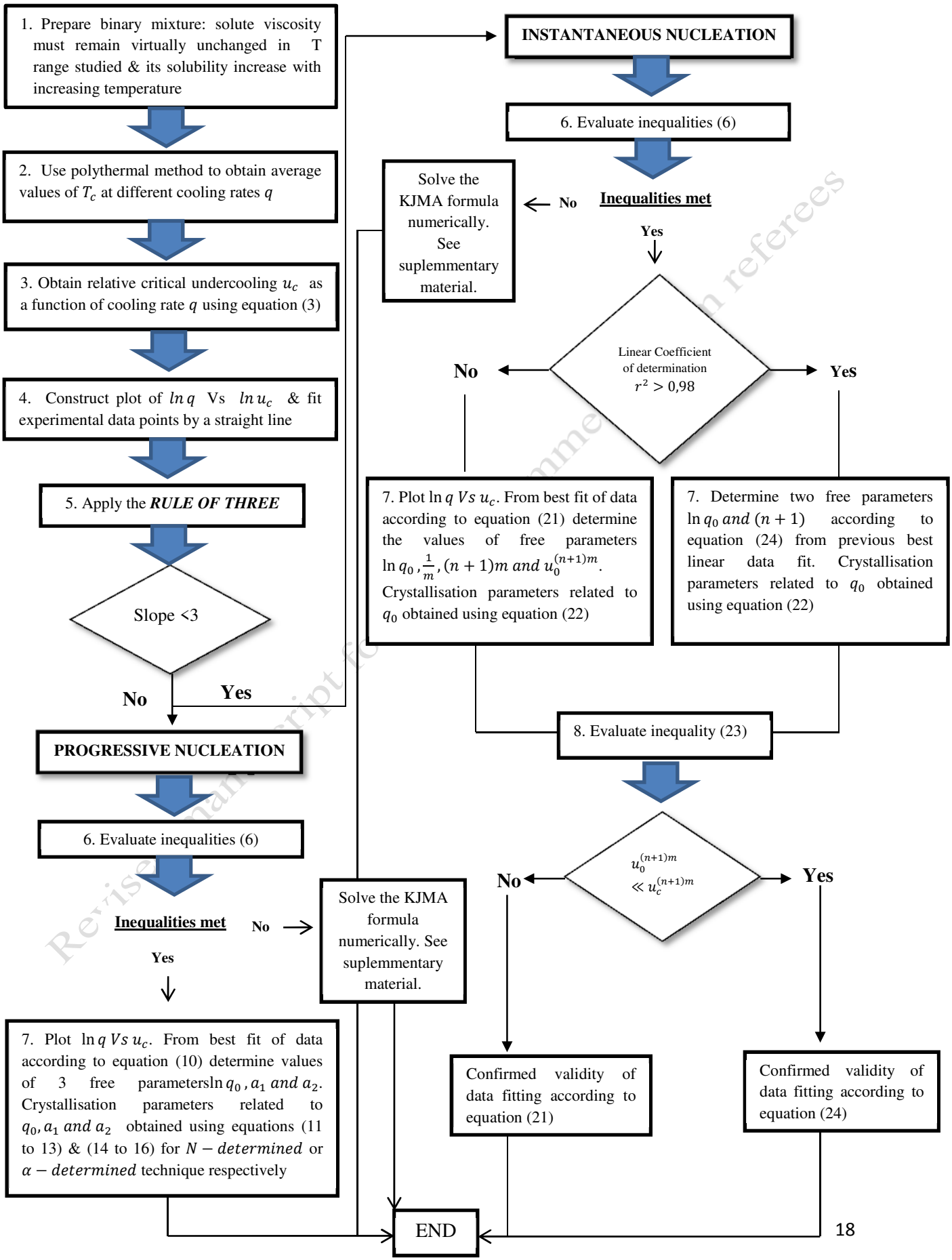

2.3 Isothermal method

Within the framework of classical theory of $3D$ nucleation, for the case of crystallisation by the polynuclear mechanism, an expression can be derived for the induction time τ as a function of the supersaturation $\Delta\mu$ which is the difference between the chemical potentials of the solute molecules in the solution and in the crystal. This expression is given by [11, 19]:

$$\tau = k_{md} e^{\frac{-\Delta\mu}{kT}} \left(1 - e^{\frac{-\Delta\mu}{kT}}\right)^{\frac{-md}{(1+md)}} \exp\left[\frac{B}{(1+md)\Delta\mu^2}\right] \tag{26}$$

Here, k_{md} is defined as

$$k_{md} = \left[\frac{(1+md)\alpha_{det}}{k_v z f_e^* C_s d_0^d f_{e,s}^{md}}\right]^{\frac{1}{(1+md)}} \tag{27}$$

where C_s is the concentration of sites in the system on which clusters of the new phase can form, f_e^* is the frequency of monomer attachment to the nucleus at $\Delta\mu = 0$, $f_{e,s}$ is the molecular attachment frequency per growth site at $\Delta\mu = 0$, $d_0 \approx \left(\frac{6v_0}{\pi}\right)^{\frac{1}{3}}$ is the molecular diameter, and z is the Zeldovich factor.

The quantities B and $\Delta\mu$ are given by:

$$B = \frac{16\pi {v_0}^2 \gamma_{eff}^3}{3kT} \tag{28}$$

$$\Delta\mu = kT \ln S \tag{29}$$

where the supersaturation ratio S is defined as:

$$S = \frac{C}{C_e} \tag{30}$$

By combining equations (26) and (29), a relationship can be established for the dependence of τ on S:

$$\ln\left\{\tau[S(S-1)^{md}]^{\frac{1}{1+md}}\right\} = \ln k_{md} + \frac{B}{(1+md)(kTln\,(S))^2} \tag{31}$$

Thus, a plot of $ln\left\{\tau[S(S-1)^{md}]^{\frac{1}{1+md}}\right\}$ vs. $\frac{1}{T^3(ln\,S)^2}$ is a straight line with a slope given by $\frac{16\pi v_0^2 \gamma_{eff}^3}{3(1+md)k^3}$

In this case, for a spherically shaped nucleus, r^* and i^*can be calculated from the equations:

$$r^* = \frac{2\gamma_{eff} v_0}{kTln\,S} \tag{32}$$

$$i^* = \frac{4\pi(r^*)^3}{3\,v_0} \tag{33}$$

2.4 Summary comments

In summary, both the polythermal and isothermal methods can be used to obtain parameters of the classical nucleation theory. In the case of the polythermal method, these parameters can be obtained with the aid of the $KBHR$ equations (10), (21) and (24) which are applicable when the critical undercooling for crystallisation by HON or $3D\ HEN$ of single-component crystallites is sufficiently small.

The following two sections include the experimental methodology and the steps required for the analysis of experimental data according to the $KBHR$ approach.

3. MATERIALS AND METHODS

3.1 Materials

Methyl stearate (96% pure) was purchased from Sigma-Aldrich, and kerosene was supplied by Infineum Ltd. The kerosene is composed of a mixture of n-alkanes, iso-alkanes and cyclo-alkanes together with aromatic hydrocarbons. The normal alkanes comprise 14.7% of the total mass with the exact distribution given in Table 1. Due to the difficulty of obtaining the composition of the other compounds by gas chromatography, their mass-percentage is not presented.

Table 1. Kerosene n-alkane mass fraction distribution as obtained by Gas Chromatography analysis

n-alkane	n-alkanes mass percentage
C8	0.19690
C9	1.00400
C10	2.99590
C11	2.44310
C12	3.29770
C13	3.11150
C14	1.49720
C15	0.31350
C16	0.04920
C17	0.02190
C18	0.01060
C19	0.00490
C20	0.00280
C21	0.00210
C22	0.00140
C23	0.00100
C24	0.00070
C25	0.00040
C26	0.00030
C27	0.00010
C28	0.00010
C29	0.00040
C30	0.00010
C31	0.00000
C32	0.00000
C33	0.00000
C34	0.00010

3.2 Experimental apparatus

Crystallisation experiments were carried out using the Avantium Crystal 16® system (see: http://www.crystallizationsystems.com/pharma/crystal16/). This provides a multiple reactor facility with four separate Peltier heated aluminium blocks, each of which has a capacity to hold four magnetically-agitated 1 ml solution vials. Each block can be individually programmed to follow a given temperature profile during which the variations in the solution turbidity are followed as a function of temperature.

The solute latent heat of crystallisation was measured using a Mettler Toledo Differential Scanning Calorimetry (DSC) 1 STAR^e system. This allowed monitoring the crystallisation transformation of individual samples placed in aluminium standard 40 µl holders.

3.3 Experimental procedure

3.3.1 Equipment calibration

In order to ensure accurate measurement of temperatures, calibration of the Crystal 16® unit was required. Four vials containing kerosene were placed in each of the blocks which were programmed to a specific temperature in the range of 20°C to -8°C. Whilst each block was kept at a chosen temperature, measurements of the actual temperature with $\pm$0.5°C accuracy were carried out by positioning a thermocouple within each of the vials. The average of the four temperatures readings obtained in each block was plotted against the programmed temperature and fitted by a straight line represented by the expression $y = 0.96x + 1.34$, which was then used to correct the experimentally measured temperature values. The temperature-calibration line obtained is given in Fig. 3.

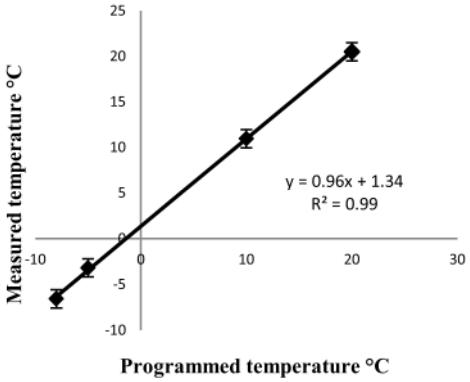

Fig. 3 Temperature calibration for the Crystal 16 unit. Temperature at which the Crystal 16® is programmed is plotted against the actual temperature of the solvent as measured by a calibrated thermocouple

3.3.2 Solutions preparation

Solutions of methyl stearate in kerosene were prepared on a 5 ml scale to equivalent solutions concentrations of 200, 250, 300 and 350 g of solute per litre of solvent, using a weighing scale of $\pm$ 0.001 g accuracy to weigh the solute and a burette of 0.1 ml accuracy to add the solvent. The solutions were stirred for half an hour with an overhead motor stirrer at 700 rpm and room temperature. Once a homogeneous liquid solution was obtained, a Fisherbrand 100-1000 μl micropipette was used to distribute the solutions in the 1 ml vials whilst for the DSC analysis a 16 mg sample corresponding to a concentration of 350 g/l was placed in a 40 µl aluminium sample holder.

3.3.3 Polythermal measurements and data analysis

The 1 ml solutions were subject to heating and cooling cycles, with each cycle initiated by heating the solutions up to 40°C where they were held for an hour to ensure complete homogenization and then cooled to 15°C where they were also held for an hour to allow equilibration. This temperature profile was applied at each solution's concentration using eight different rates 0.25, 1, 3.2, 5, 7, 9, 11 and 13 °C/min which were used in both the

heating and cooling segments. At each rate the temperature cycle was repeated ten times to obtain average values for the crystallisation and dissolution temperatures T_c and T_{diss}. This approach was important in terms of improving the data fitting and minimising the standard deviation (SD) of the crystallisation temperatures T_c. Fig. 4 shows a typical experimental profile together with a representative raw data set for one of the experimental runs.

The crystallisation and dissolution temperatures were estimated based upon the points in the turbidity profile at which sudden changes in light transmittance are detected. The crystallisation temperatures were taken as the points at which the light transmittance was found to decrease by at least 10% and the dissolution temperature as those points at which the light transmittance has reached at least 20%.

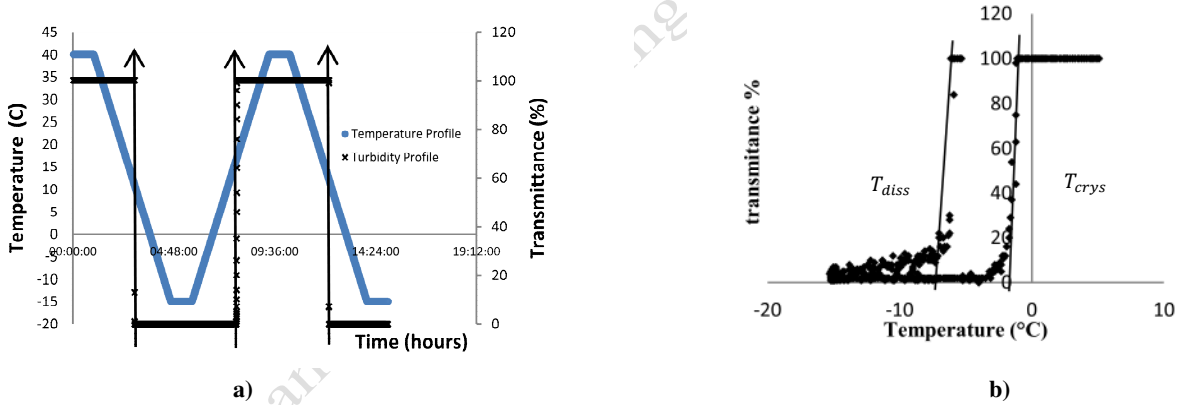

Fig. 4 a) Typical experimental profile using Crystal 16® by applying the polythermal method. b) Representative turbidity profile in transmittance vs. temperature coordinates obtained by the application of a polythermal method

The $KBHR$ approach was applied to the process and used to analyse the polythermal data. At each concentration the average values of the dissolution and crystallisation temperatures were plotted as a function of cooling rate q. These data points were then fitted by straight lines to obtain the interrelationship of the $MZSW$ as a function of the cooling rate. The solubility-supersolubility curves were constructed out of the extrapolation of these lines to zero cooling rate from which the associated values of T_{diss} and T_c were determined. The extrapolation of

the T_{diss} lines delivering the solution equilibrium temperature T_e. Fig. 5 gives an example of the extrapolation of the best linear fit to $T_{diss}(q)$ and $T_c(q)$ data points for a concentration of 200 g/l.

Using equation (2), at each concentration and cooling rate the critical undercooling ΔT_c was calculated from the average of the experimental crystallisation temperatures T_c and the corresponding solution equilibrium temperatures T_e. Then the relative critical undercooling u_c was obtained from equation (3).

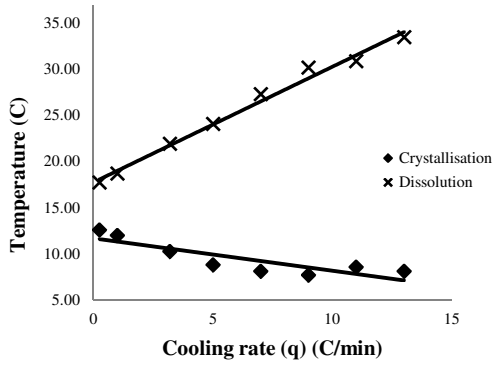

Fig 5. Extrapolation to zero cooling rate of the best linear fit of $T_{diss}(q)$ and $T_c(q)$ data points for a concentration of 200 gr/l. The best linear fits are represented by expressions $y = 1.25x + 17.77$ and $y = -0.35x + 11.67$ for $T_{diss}(q)$ and $T_c(q)$ respectively.

For each concentration, a plot of $u_c(q)$ data in $ln - ln$ coordinates was obtained and the data points fitted to a straight line from which the numerical value of the slope was used to assess the nucleation mechanism governing the process.

Following this, the data were analysed using the procedure summarised in Fig. 2 and the effective interfacial tensions γ_{eff} for the crystallite nucleus determined. Numerical values for r^* and i^* were calculated using equations (17) and (18), respectively.

3.3.4 Isothermal measurements and data analysis

Supersaturation values used for the isothermal methodology were chosen with reference to the characterization of the $MSZW$ determined using the solubility-supersolubility relationship given in Fig. 6. For each solution concentration four different temperatures within the $MSZW$ were chosen to carry out the isothermal crystallisation experiments. The $MSZW$ was typically about 6ºC (see figure 7). However, the measured induction times at temperatures corresponding to lower undercooling values were too long for practical measurements and so the data was obtained within a small temperature range (12-12.8ºC, 14-14.8ºC, 17-18ºC and 17.8-18.5ºC for 200, 250, 300 and 350 g/l, respectively), see tabulated values given in Table 7.

The 1 ml solutions were heated up to 10°C above the corresponding solute dissolution temperature, in this case 28, 30, 32 and 33 °C for 200, 250, 300 and 350 g/l respectively. The solutions were held for an hour at this temperature to ensure homogenization, and then rapidly cooled down at a constant rate of 10°C/min, down to the chosen temperature within the $MSZW$, where the supersaturated solutions were maintained and stirred until the onset of crystallisation was detected. The induction time τ was monitored by the change in the solution turbidity, from the time at which the solution reached the predetermined temperature to that of the crystallisation onset, which corresponds to the time at which the light transmittance decreased by at least 10%. For each concentration, four different temperatures were used together with four repeat measurements at each of the chosen temperatures. Fig. 6 shows an experimental temperature profile from one of the runs together with a representative raw data set.

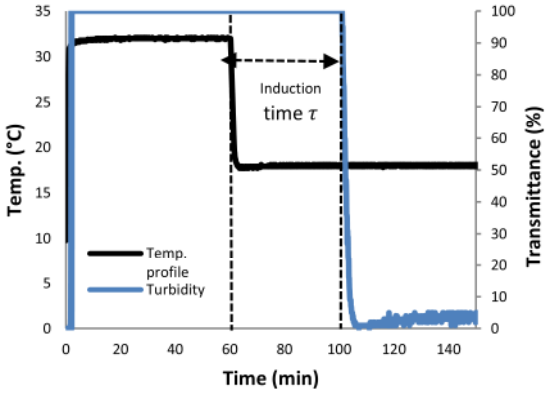

(a)

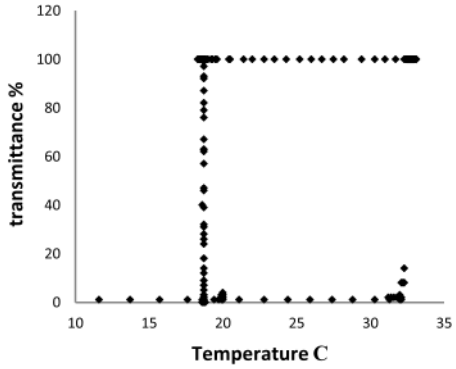

(b)

Fig. 6 a) Crystal 16® typical experimental profile obtained by the application of the isothermal method b) Representative turbidity profile in transmittance vs temperature coordinates obtained by the application of the isothermal method

For each solution concentration, the average induction times τ for each of the chosen temperatures T were plotted in $\ln\left\{\tau[S(S-1)^{md}]^{\frac{1}{1+md}}\right\}$ vs $\frac{1}{T^3(\ln S)^2}$ coordinates and fitted by a straight line. The slopes of the lines were then used to obtain the effective interfacial tensions γ_{eff} according to equation (31). The values of r^* and i^* were calculated using equations (32) and (33) respectively.

3.3.5 *DSC* measurements and data analysis

The sample was subject to a temperature profile initiated by heating the solution up to 40°C where it was held for an hour to ensure complete homogenization and then cooled to -15°C where it was also held for an hour to allow equilibration. A constant rate of 0.25°C/min was used in both the heating and cooling segments. The temperature cycle was repeated five times to obtain average values for the solute heat of crystallisation obtained from the integration of the corresponding exothermic peaks.

4. RESULTS AND DISCUSSION

4.1 Polythermal data

The polythermal data were processed to obtain the solubility-supersolubility curves and nucleation parameters by applying the $KBHR$ approach. The average values for the collected crystallisation and dissolution temperatures and their standard deviations SD together with the critical undercooling ΔT_c at the corresponding concentrations and cooling rates are presented in Table 2. The correlation coefficients R^2 for the $T_{diss}(q)$ lines used to obtain equilibrium temperature T_e are presented in Table 4.

Fig. 7 shows the data points obtained for the equilibrium dissolutions and crystallisation temperatures at each concentration as described in detail in Section 3. The solubility-supersolubility lines were plotted by fitting these data points using an exponential regression which in the case of the solubility curve delivers an expression of the form $y = 31.65e^{0.1037x}$.

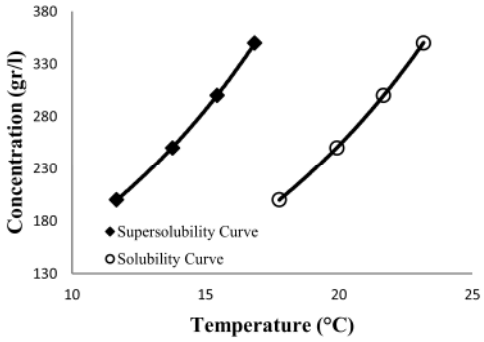

Fig. 7 Solubility-supersolubility curve of methyl stearate in kerosene. Supersolubility curve data points obtained by extrapolating to the Y-axis the best linear fit of cooling rate q vs. crystallisation temperature T_c of the data obtained by the polythermal method at each concentration. Solubility curve data points obtained by extrapolating to the Y-axis the best linear fit of cooling rate q vs. dissolution temperature T_{diss} of the data obtained by the polythermal method at each concentration

For each concentration, the results of the relative critical undercooling u_c calculated at each cooling rate q are given in Table 3. The $u_c$values are within the limits specified by inequalities (6). This means that in all cases the experimentally obtained limit of metastability corresponds to a relatively low supersaturation for which the use of the $KBHR$ approach is justified.

For each concentration a plot of cooling rate q vs. relative critical undercooling u_c in *ln-ln* coordinates was then constructed to obtain the slope of the straight line fitting these data points. Fig. 8 presents the plot obtained for a concentration of 200 g/l for which the best linear fitting to the data is given by $y = 5.17x + 15.76$. The slope and the correlation coefficient R^2 of the best-fit straight line to the data at each concentration are presented in Table 4.

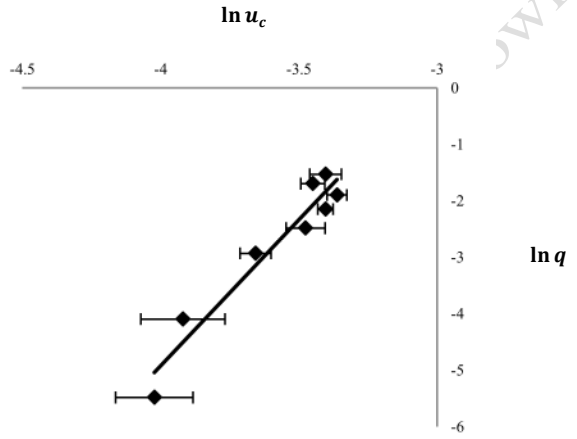

Fig. 8 Plot of experimental data in $ln\ q$ Vs $ln\ u_c$ coordinates for methyl stearate in kerosene at a concentration of 200 g/l

In all cases the slopes of the lines are higher than 3, suggesting that crystallisation of methyl stearate in solution with kerosene proceeds via the PN mechanism. Thus, according to the $KBHR$ approach, equation (10) should describe the experimental data plotted in $Ln\ q$ vs. u_c

coordinates as detailed in the procedure to apply the $KBHR$ approach given in Fig. 2. To obtain the parameters a_1, a_2 and $ln\, q_0$, the fit of this equation to the experimental data was done using OriginPro 8.5.1. through a nonlinear least-square method . The values of these parameters for each of the solution concentrations and the correlation coefficients for the fitting of equation (10) to the experimental data are presented in Table 4.

The best-fit curves that minimises the sum of squares of the deviations between the experimental $u_c(q)$ values and those calculated from equation (10) were obtained by setting $a_1 = 3$. An example of such a curve for the concentration of 200 g/l is presented in Fig. 9.

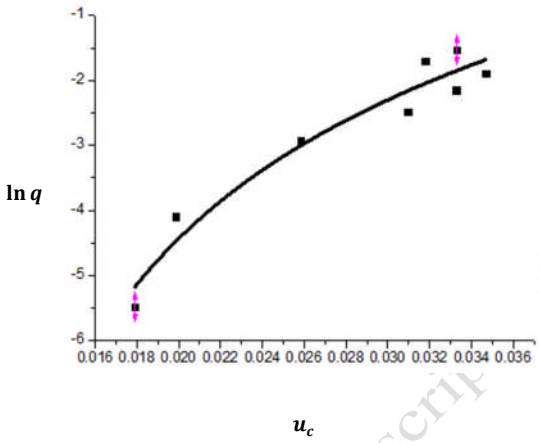

Fig. 9 Increase in relative critical undercooling with the natural logarithm of cooling rate. The points represent the data for crystallisation of methyl stearate in solution with kerosene 200 g/l; the line illustrates the best fit according to equation (10)

Table 2. Average dissolution and crystallisation temperatures as a function of cooling rate for methyl stearate in kerosene at solution concentrations 200, 250, 300 and 350 g/l. Standard deviation of crystallisation and dissolution temperatures. Critical undercooling ΔT_c calculated according to equation (2). Equilibrium temperatures T_e obtained from extrapolation of best-fit straight lines through $T_{diss}(q)$ data points.

Rate ℃ /min	T_c (℃)	$SD\ T_c$ (℃)	T_{diss} (℃)	$SD\ T_{dss}$ (℃)	ΔT_c
200 g/l					
0.25	12.56	0.72	17.69	0.08	5.21
1	11.99	0.87	18.66	0.07	5.77
3.2	10.26	0.44	21.92	0.28	7.51
5	8.77	0.63	24.07	0.48	9.00
7	8.10	0.28	27.29	0.65	9.67
9	7.68	0.36	30.16	0.78	10.08
11	8.53	0.40	30.85	1.58	9.24
13	8.09	0.56	33.46	1.38	9.68
			T_e=17.77		
250 g/l					
0.25	14.88	0.63	19.59	0.09	5.04
1	14.16	0.84	20.81	0.18	5.76
3.2	12.15	0.50	24.85	0.39	7.78
5	10.82	0.41	28.49	0.42	9.10
7	10.27	0.54	31.88	0.67	9.66
9	9.09	1.00	34.12	0.96	10.83
11	10.49	0.49	36.30	2.04	9.44
13	10.54	0.30	38.78	0.46	9.38
			T_e=19.93		
300 g/l					
0.25	16.54	0.48	21.03	0.06	5.12
1	15.29	0.45	22.46	0.18	6.38
3.2	13.96	0.50	26.87	0.44	7.70
5	12.95	0.43	29.88	0.81	8.71
7	11.53	0.49	33.68	0.66	10.13
9	10.82	0.55	35.88	0.85	10.84
11	11.66	0.53	37.30	1.59	10.01
13	11.80	0.34	40.03	0.52	9.86
			T_e=21.66		
350 g/l					
0.25	17.75	0.47	22.19	0.10	5.42
1	16.85	0.28	23.71	0.18	6.32
3.2	15.12	0.50	28.29	0.53	8.05
5	14.33	0.45	31.44	0.93	8.84
7	13.31	0.42	35.36	0.81	9.86
9	11.69	0.31	37.52	0.94	11.48
11	12.86	0.40	38.96	1.34	10.31
13	12.91	0.45	40.12	0.38	10.26
			T_e=23.17		

Table 3. Relative critical undercooling u_c as a function of concentration and cooling rate for solution of methyl stearate in kerosene

	u_c			
Cooling rate $q\ \left(\frac{K}{s}\right)$	200 g/l	250 g/l	300 g/l	350 g/l
0.004	0.018	0.017	0.017	0.018
0.017	0.020	0.020	0.022	0.021
0.053	0.026	0.027	0.026	0.027
0.083	0.031	0.031	0.030	0.030
0.117	0.033	0.033	0.034	0.033
0.150	0.035	0.037	0.037	0.039
0.183	0.032	0.032	0.034	0.035
0.217	0.033	0.032	0.017	0.035

Table 4. Saturation temperatures and corresponding correlation coefficients of the best linear fitting of $T_{diss}(q)$ data; slopes of the best linear fit to data points in $ln\ q$ vs. $ln\ u_c$ coordinates and correlation coefficients; values of the free parameters a_1, a_2 and $ln\ q_o$ obtained from the data fitting in $ln\ q$ vs. u_c coordinates according to equation (10) and correlation coefficients (the values are for solution concentrations of 200, 250, 300, and 350 g/l, and the errors of the slope and the free parameters refer to the 95% confidence interval).

Con. (g/l)	$T_e(K)$	R^2, fitting $T_{diss}(q)$	Slope of best-fit straight line of $\ln u_c\ vs. \ln q$	R^2, linear fitting	Nucleation Mechanism	a_1	$a_2 = b$	$\ln q_0$	$q_0\left(\frac{K}{s}\right)$	R^2, fitting equation (10)
200	290.77	0.99	5.17±0.57	0.93	PN	3	0.0006535±1.48*10^{-4}	8.966±0.25	7834.0	0.94
250	292.93	0.99	4.82±0.59	0.92	PN	3	0.0005428±1.47*10^{-4}	8.806±0.26	6673.5	0.93
300	294.66	0.98	5.05±0.47	0.95	PN	3	0.0006291±1.132*10^{-4}	8.826±0.19	6811.2	0.97
350	296.17	0.96	5.06±0.51	0.94	PN	3	0.0006976±1.26*10^{-4}	8.819±0.20	6761.1	0.96

As in all cases a_1 is set equal to 3, equations (12) and (13) can be used to proceed further. According to equation (12) a_2 equals b, a dimensionless thermodynamic parameter defined by equation (9) from which the γ_{eff} can be calculated. The results obtained for $\ln q_0$ yield the values of q_o, a parameter related through equation (13) to the nucleation rate constant K_J and the number N_{det} of crystallites at the detection point.

The effective interfacial tension γ_{eff} was evaluated from equation (9), using $v_o = 0.491\ nm^3$ [20], the calculated equilibrium temperatures T_e, the shape factor $k_n = \frac{16}{3}\pi$ for spherical nuclei and the molecular latent heat λ of crystallisation estimated to be $8.98\ x\ 10^{-20}\ J$ from measurements of the solute heat of crystallisation using DSC. Also, the critical nucleus radius r^* and number i^* of molecules at $u_c = 0.017$ and 0.035, the lowest and the highest experimentally determined relative critical undercoolings, were calculated from equation (17) and (18) respectively. The values obtained are given in Table 5.

Table 5. Interfacial tension, critical radius and number of molecules for nucleation of methyl stearate in kerosene at four solution concentrations (the Critical radius and number of molecules are calculated at $u_c = 0.035$ and 0.017) .

Concentration (g/l)	$\gamma_{eff}\ (mJ/m^2)$	$r^*(nm)$	i^*
200	1.74	0.54-1.12	1-12
250	1.64	0.51-1.05	1-10
300	1.72	0.54-1.11	1-12
350	1.79	0.56-1.15	1-13

A comparison of the correlation coefficients R^2 and the errors of the parameters shows that a better fit is obtained when a non-linear regression is applied, a result that should be expected in the scope of the $KBHR$ approach according to which the dependence of the critical undercooling on the cooling rate is not linear. It has been shown [1] that only in a sufficiently narrow q range $ln\ u_c$ and $\ln q$ are approximately linearly related, with the slope revealing the governing nucleation mechanism. A more elaborate statistical analysis comparing the goodness of the fitting models to describe the experimental $u_c(q)$ data reinforces the suitability of using equation (10) of the $KBHR$ approach for the polythermal data analysis. The standard deviations SD and covariance of the parameters in the two models are presented in Table 6.

Table 6. Standard deviation and covariance of the parameters in the linear regression model according to equation (25) and the parameters in the regression model according to equation (10)

Linear Fitting according to equation (25)						
Concentration (g/l)	Slope Standard Deviation (SD)	Intercept Standard Deviation (SD)	Covariance Slope-Intercept			
200	1.48	5.33	7.89			
250	1.39	5.00	6.95			
300	1.43	5.12	7.33			
350	1.44	5.12	7.38			
Fitting according to equation (10)						
Concentration (g/l)	$\ln q_0$ Standard Deviation (SD)	a_1 Standard Deviation (SD)	a_2 Standard Deviation (SD)	Covariance $\ln q_0 - a_1$	Covariance $\ln q_0 - a_2$	Covariance $a_1 - a_2$
200	34.42	10.92	0.0032	375.79	-0.11	-0.03
250	24.47	11.99	0.0034	453.88	-0.13	-0.04
300	22.63	11.16	0.0033	391.36	-0.11	-0.04
350	26.17	10.24	0.0032	326.06	-0.10	-0.03

A relatively high standard deviation is observed for the fitting according to equation (10), which also has an influence on the values of the covariance between the parameters $ln\ q_0$ and

a_1. However the covariance is very low in all other cases. This suggests that the model according to equation (10) provides a good fit to the collected polythermal experimental data and can be used to proceed with further calculations.

The low values of the effective interfacial tension are an indication of a prevalence of HEN mechanism for the nucleation of the methyl stearate crystallites. These values have the order of magnitude of those reported earlier for HEN of m-ABA and L-His [21] and are very similar to those of other organic molecules such as eflucimibe [22], paracetamol [23], ketoprofen [24] and n-alkanes [25-28]. In the latter case, although some of the values are lower, there are others that are equivalent or very close to those obtained for methyl stearate crystals, as in the case of the interfacial tensions reported for $C_{20}H_{42}/C_{21}H_{44}$ and $C_{20}H_{42}/C_{22}H_{46}$ solute mixtures in solution with dodecane (see Table 10).

Through the use of equation (13), the nucleation rate constant could also be estimated but this requires the corresponding values of N_{det}, the number of crystallites formed at the detection point, for which additional experimental work would be necessary. We are aiming to collect these data and report them in a future publication along with the corresponding crystal nucleation and growth rates, which will extend the application of the $KBHR$ approach.

The collection of all data presented above was not an easy task, as it required running 320 temperature cycles, each of which can last an average of three hours. Thus, a sensitivity analysis for the applied experimental methodology was carried out. Three additional scenarios were used with the aim of assessing the influence that reducing the number of cooling rates and/or temperature cycles would have on the parameters obtained by applying the $KBHR$ approach. It was found that reasonable interfacial tension values were still

obtained even by a 50% reduction of the number of both the cooling rates and the T_c measurements. This analysis suggests that a reduced data set of four cooling rates q and five temperature cycles at each cooling rate would be sufficient for this work[*]. The experimental data were also analysed using the empirical Nyvlt approach. These results showed that the slopes of the lines obtained from best linear fit to the experimental data by employing the Nyvlt linearization can be 1.5 to 2.5 times lower than those obtained by best fit to the data in the coordinates corresponding to the $KBHR$ approach[*]

4.2 Isothermal data and comparison with the polythermal results

The analysis of the data for the induction time τ data as a function of the supersaturation ratio S was carried out in order to calculate nucleation parameters and compare them with those obtained by the analysis of the polythermal data. The average values of τ obtained as a function of S and the solution concentration are given in Table 7.

At each concentration, a linear dependence of $\ln\left\{\tau[S(S-1)^{md}]^{\frac{1}{1+md}}\right\}$ on $\frac{1}{T^3(\ln S)^2}$ was found with assumed $m = 0.5$ and $d = 2$, values corresponding to diffusion-controlled crystallite growth in two dimensions of space [11]. The choice of the d value is supported by pictures of methyl stearate crystals obtained experimentally, in which a plate-like morphology was observed. Interfacial tensions were calculated from the slopes of the straight lines predicted by equation (31). Fig. 10 shows an example of the plot obtained for a

[*] Details of the sensitivity analysis are presented in Section 2 of the supplementary material.
[*] Analysis of the experimental data using the Nyvlt approach along with a useful expression that relates the slopes of the experimental data linearization using the Nyvlt and the $KBHR$ approaches is presented in Section 3 of the supplementary material.

concentration of 200 g/l for which the best linear fit to the data is represented by $y = 6 * 10^7 x - 1.74$.

Table 7. Induction time as a function of supersaturation ratio for solutions of methyl stearate in kerosene. Solutions of 200, 250, 300, 350 g of solute per litre of solvent cooled to four holding temperatures within the corresponding metastable zone.

$T(°C)$	$T(°K)$	*Average Induction time* (τ)(sec)	*Equilibrium concentration* C_e $(\frac{g}{l})$ *at the holding temperature*	*Supersaturation ratio* (S)
200 g/l				
12	285	240	109.87	1.57
12.3	285.3	675	113.34	1.54
12.5	285.5	915	115.72	1.51
12.8	285.8	3525	119.37	1.48
250 g/l				
14	287	345	135.19	1.60
14.3	287.3	600	139.46	1.56
14.5	287.5	2385	142.39	1.54
14.8	287.8	2430	146.89	1.50
300 g/l				
17	290	405	184.53	1.45
17.3	290.3	315	190.36	1.42
17.5	290.5	825	194.35	1.39
18	291	1395	204.69	1.34
350 g/l				
17.8	290.8	1155	200.49	1.52
18	291	2250	204.69	1.50
18.3	291.3	2505	211.16	1.46
18.5	291.5	4200	215.58	1.44

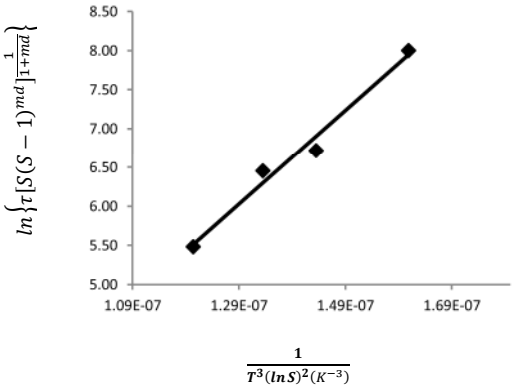

Fig. 10 Linear fit of experimental $\tau(S)$ data plotted in $ln\left\{\tau\left[S(S-1)^{md}\right]^{\frac{1}{1+md}}\right\}$ vs. $\frac{1}{T^3(lnS)^2}$ coordinates (solution concentration of 200 g/l).

The calculated values of γ_{eff}, $r^*$and i^* are presented in Table 8 together with the values obtained by the polythermal method.

Table 8. Slopes of the best linear fit of experimental data plotted in $ln\left\{\tau\left[S(S-1)^{md}\right]^{\frac{1}{1+md}}\right\}$ vs. $\frac{1}{T^3(ln\,S)^2}$ coordinates and corresponding correlation coefficient, effective interfacial tension γ_{eff}, critical nucleus radius r^* and number i^* of molecules for nucleation of methyl stearate in kerosene at different concentrations. (r^* and i^* are given for the S values corresponding to $u = 0.035$ and 0.017, and the errors of the slope refer to the 95% confidence interval).

Con g/l	*Slope of the best linear fit of the experimental data plotted in* $ln\left\{\tau[S(S-1)^{md}]^{\frac{1}{1+md}}\right\}$ *Vs* $\frac{1}{T^3(Ln\,S)^2}$ *coordinates*	R^2	$\gamma_{eff}\left(\frac{mJ}{m^2}\right)$ *Isothermal method*	$r^*\,(nm)$ *Isothermal method*	i^* *Isothermal method*	$\gamma_{eff}\left(\frac{mJ}{m^2}\right)$ *Polyhermal method*	$r^*\,(nm)$ *Polyhermal method*	i^* *Polythermal method*
200	(3±0.60)*10^7	0.98	3.39	1.08-2.18	11-89	1.74	0.54-1.12	1-12
250	(3±1.92)*10^7	0.80	3.39	1.05-2.12	10-81	1.64	0.51-1.05	1-10
300	(7±4.89)*10^6	0.74	2.09	0.64-1.28	2-18	1.72	0.54-1.11	1-12
350	(1±0.70)*10^7	0.86	2.35	0.72-1.46	3-27	1.79	0.56-1.15	1-13

A comparison of the parameter values shows that in all cases γ_{eff}, $r^*$and i^* calculated by means of the isothermal method are greater than those obtained by means of the polythermal method but are of the same order of magnitude. "The isothermal" γ_{eff} and r^* values are approximately 2, 2, 1.2 and 1.3 times greater than the "polythermal" ones for 200, 250, 300 and 350 g/l, respectively. These differences are reflected in a more noticeable increase of the critical nucleus number i^* of molecules obtained by means of the isothermal method where, for the lower concentrations of 200 and 250 g/l, it is between 7 and 11 times greater than that obtained by the polythermal method. However, for the higher concentrations of 300 and 350 g/l, the i^*values are only in the range of 1.5 to 3 times greater than those obtained by the polythermal method. For these concentrations, although the values of i^* calculated from the isothermal data are still greater than those obtained from the polythermal data, in both cases they are still in the range of typical values for HEN, well below 50 molecules.

It is important to notice that the supersaturation range in which crystallisation was detected through the polythermal analysis is considerably wider than that used to assess induction

times through the isothermal method. This is so, because in the latter case the supersaturations where chosen within the $MSZW$ defined by the extrapolation to zero cooling rate of the $T_{diss}(q)$ and $T_c(q)$ dependences, which give a $MSZW$ limited by higher crystallisation temperatures. This fact might explain the differences in the parameter values in the case of the lower solution concentrations for which two different nucleation mechanisms in the temperatures range of study may be present. However, to verify this assumption the use of a wider supersaturation range in the isothermal data analysis would be needed.

To further analyse these data, it is useful to determine the theoretical values of the interfacial tension γ for HON, which can be obtained with the aid of the Stefan-Skapski-Turnbull expression corresponding to spherical nuclei and given by [11, 29] :

$$\gamma = 0.514kT\frac{1}{{v_0}^{2/3}}\ln\frac{1}{N_a v_o C_e} \tag{34}$$

where N_a is Avogadro´s number, and C_e is the molar solubility.

The nucleation-activity factors (ψ) that control the value of the effective interfacial tension γ_{eff} can be calculated with the help of the formula

$$\gamma_{eff} = \psi\gamma \tag{35}$$

Table 9 lists the γ and ψ values obtained from equations (34) and (35) with the help of the γ_{eff} values calculated by both the polythermal and the isothermal method, using the corresponding molar solubility at $u = 0.035$ and 0.017.

Table 9. Interfacial tension for HON and nucleation-activity factor for $3D$ HEN as a function of solution concentration.

$Con\ (g/l)$	$\gamma\left(\frac{mJ}{m^2}\right)$	ψ $from\ polythermal\ data$	ψ $from\ isothermal\ data$
200	7.24-8.42	0.24-0.21	0.47-0.40
250	6.73-7.95	0.24-0.21	0.50-0.43
300	6.32-7.59	0.27-0.23	0.33-0.28
350	5.99-7.24	0.30-0.25	0.39-0.32

Table 9 shows that for all concentrations the values of the nucleation-activity factor resulting from both the polythermal and isothermal analysis are well below the theoretical value of unity for HON. This indicates that HEN is the dominating mechanism controlling the methyl stearate formation in the whole temperature range studied.

The differences in the values of the nucleation parameters obtained by either the polythermal or the isothermal method could be attributed to the experimental methodology applied in the isothermal method. It was observed that induction time results are not very reproducible and repeatable and can vary significantly, even under the same experimental conditions, thus reflecting the stochastic nature of the nucleation process. The correlation coefficients for all concentrations show that a straight line does not fit the experimental data very well. As previously suggested by ter Horst and Jiang [21], to obtain accurate results from the application of the isothermal method, a probability distribution of the induction times at constant supersaturation ratio S should be constructed. To do that, however, an appreciable amount of time has to be spent for collecting the required experimental data, because a minimum of five values of the supersaturationn ratio S and eighty measurements of the induction time at each S value are suggested.

A comparative summary of interfacial tensions previously reported for organic compounds and the interfacial tensions obtained from both the polythermal and the isothermal methods is presented in Table 10.

Table 10. Previously reported values of interfacial tensions of some organic compounds and values obtained for the crystallisation of methyl stearate from kerosene by both the polythermal and the isothermal methods.

Compound	Reported γ $\left(\frac{mJ}{m^2}\right)$
$m-ABA$ in water ethanol mixture $m-His$ in water ethanol mixture [21]	8.7 5.1
Eflucimibe in ethanol and n-heptane mixture Polymorph A Polymorph B [22]	 5.17 4.23
Paracetamol in acetone-water mixtures [23]	1.4-2.8
Ketoprofen in acetone [24]	1.47
Liquid alkanes $C_{17}H_{36}$ $C_{18}H_{38}$ $C_{24}H_{50}$ [25]	 7.20 9.64 8.20
Solutions of $C_{20}H_{42}$ + impurities (n-alkanes from $n-C_{18}$ to $n-C_{22}$) in Dodecane $C_{20}H_{42}$ $C_{20}H_{42}/C_{18}H_{38}$ $C_{20}H_{42}/C_{19}H_{40}$ $C_{20}H_{42}/C_{21}H_{44}$ $C_{20}H_{42}/C_{22}H_{46}$ [26]	 0.389 0.775 0.844 1.713 1.170
$C_{22}H_{46}$ in Dodecane Mole fraction 10% Mole fraction 15% Mole fraction 20% [27]	 0.493 0.217 0.315
$C_{24}H_{50}$ in Decalin 2% mole fraction 7% mole fraction 19% mole fraction $C_{24}H_{50}$ in Dodecane. (two Different nucleation mechanisms observed) HON 1% mole fraction 5% mole fraction 19% mole fraction HEN 1% mole fraction 5% mole fraction 19% mole fraction [28]	 0.69 0.64 0.29 0.86 0.74 0.49 0.49 0.45 0.29
Methyl stearate in kerosene (Polythermal method) 200 g/l 250 g/l 300 g/l 350 g/l	 1.74 1.64 1.72 1.79
Methyl stearate in kerosene (Isothermal method) 200 g/l 250 g/l 300 g/l 350 g/l	 3.39 3.39 2.09 2.35

4.3 Potential for further model development

The main advantage of the $KBHR$ approach is that it provides a quantitative account of the influence of cooling rate on the overall crystallisation process and hence provides an insight into the crystallite nucleation and growth mechanisms involved. The use of the complete set of expressions presented in this paper can deliver parameters such as e.g.: the nucleation rate constant K_N, the nucleus effective interfacial tension γ_{eff}, the crystal growth rate constant K_G and the crystallite growth exponents m and n. Additionally, the crystallites´ nucleation and growth rates could also be obtained by using these parameters in the respective formulae of the classical nucleation theory and the crystallite growth theories that model the temporal increase of crystallite radius through different mechanisms. The use of the mechanism-specific crystallite growth rate expressions presented by D. Kashchiev and A. Firoozabadi [18] will be addressed in future work.

Critically, the $KBHR$ approach provides a rational alternative to existing approaches based on empirical models. However, this approach is derived by making use of traditional expressions that rely on a number of simplifications and therefore there is more that could be done in the future, specifically to address the underlying molecular-scale interactions which are bound to be involved in directing and controlling the nucleation process [30, 31]. Clearly, an understanding of the nucleation kinetics at the molecular level is also required. In particular, the interactions between moieties or functional groups associated with the molecular building blocks of a nucleus known as "synthons", need to be integrated within the model, and through this assess the relative balance between the bulk (intrinsic) synthons, which are fully co-coordinated in the crystallographic structure and the under-saturated surface (extrinsic) synthons which are present at the crystallite/solution interface. The latter will be much less co-coordinated to other solute molecules due to competition with solvent molecules. These

synthons can be expected to provide the driving force for crystallisation processes such as crystallite nucleation and growth. A "synthonic engineering" approach has obvious value in that through it the initial stages associated with the molecular assembly of materials can be understood and quantified. This is especially useful in addressing the nature of complex surface properties and the inherent anisotropy of many compounds, particularly those which crystallise in low symmetry structures. This is the case for many industrial materials such as fuels, confectionery products, pharmaceuticals and fine chemicals. In this regard, the shape of the particle needs further quantification, in a manner which draws down on the now comparatively routine application of the molecular modelling of dimers [32, 33], clusters [34-38], surfaces [30, 39, 40], point defects and additives [41-45] action on crystallisation. Such molecular scale modelling can be expected to have an impact e.g. using morphological modelling in the calculation of the volume of crystallites through the $KBHR$ approach. Similarly, the use of the classical nucleation theory for derivation of some of the expressions presented implies interfacial tension corresponding to the crystal equilibrium form, whereas in practice this parameter can vary significantly between the crystallographic forms that are present in the external crystal morphology. In this case, molecular modelling using grid search methods can be used to examine molecule/surface binding and to calculate the interfacial tensions as a function of solution composition [30, 39, 40]. This has been achieved through characterising the strength of the various surface-specific (extrinsic) synthons that contribute to the growth of the different habit faces [35], i.e.

$$\gamma_{particle} = \frac{\sum_{i=1}^{N} M_{i(hkl)} A_{i(hkl)} \gamma_{i(hkl)}}{A_{total}} \quad (36)$$

where N is the number of crystallographic forms (hkl) displayed in the external crystal morphology, $M_{i(hkl)}$ is the multiplicity of these individual forms, $A_{i(hkl)}$ is their surface area, $\gamma_{i(hkl)}$ is their interfacial tension and A_{total} is the total surface area of the crystal.

This approach could be applied, e.g., to segment the calculated interfacial tensions as obtained from the $KBHR$ model, to yield the inter-relationship between nucleus shape and surface chemistry with the resulting interfacial tensions derived for the individual crystal habit planes [30, 39]. This is valuable given, its potential application through the use of the Gibb-Thompson expression, to calculate solubility enhancement as a function of reduced crystal size [40]. Such an approach can also be integrated with morphology prediction, with the potential to provide a more rigorous implementation of the model presented here, particularly in terms of defining a methodology for predicting the influence of crystallisation environment on the crystal growth rate [39, 41-44].

Molecular cluster modelling also provide a useful predictive way for modelling the stability of different polymorphs as a function of their crystal size. Linking this approach to the prediction of cluster size through the study presented in this paper, is potentially valuable in terms of being able to predict the correct crystallisation supersaturation needed to generate the required cluster size and thus, through this, to design the crystallisation processes needed to direct the polymorphic form desired [35, 37, 38].

A key future challenge, in terms of molecular scale predictions of nucleation behaviour, lies perhaps in trying to understand the inter-relationship (child-adult) between the incipient "crystal structure" present in the post-nucleation clusters (child) in relationship to that present in the fully formed micro/macro scale crystal structure (adult). For example, a sharp deviation

between the structures of the material at the nanoscale with respect to that present in the bulk crystal structures could be taken to be indicative of a material's ease of crystallisation or "crystallisability". Aspects of this, have been recently addressed regarding the understanding of the crystallisability of L-glutamic acid and D-mannitol [35], and this work forms one of the focus areas in our current research.

5. CONCLUSIONS

A methodology was developed to assess the mechanisms and the kinetics associated with solutions crystallisation. This methodology makes use of the recently developed $KBHR$ approach in which polythermal experimental data are analysed to deliver important parameters of the kinetics of solutions crystallisation that otherwise could only be obtained by combined application of the isothermal and polythermal methods. This is particularly important, as obtaining these parameters in the case of the isothermal method is stymied by the stochastic nature of nucleation which manifests itself in the large variation of the induction time for crystallisation.

A model system, methyl stearate crystallising from kerosene solutions, was used to test the developed methodology. The results obtained indicate that the crystallisation of methyl stearate in kerosene takes place by heterogeneous PN, i.e. the crystal nuclei are formed progressively on nucleation-active sites. The inferred values of the effective interfacial tensions are from 1.64-1.79 $\frac{mJ}{m^2}$ for solution concentrations in the range of 200 to 350 g/l respectively.

The application of the methodology can be extended to obtain additional crystal nucleation and crystal growth rate parameters but this requires the collection of additional experimental data for which future work is planned.

ACKNOWLEDGMENTS

The authors gratefully acknowledge Infineum Ltd. for the funding of this research which forms part of the doctoral studies of one of us (D.C.). We are also most grateful to Avantium Technologies for the loan of a Crystal 16 automated crystallisation system and their advice related to its application in this work.

The underpinning concepts presented in this paper were developed through a visiting professorship awarded to one of us (D.K.) in the Institute of Particle Sciences and Engineering at the University of Leeds, with the financial support of the Leverhulme Trust (Grant F10100A).

We also gratefully acknowledge the UK´s EPSRC for the support of nucleation research at Leeds and Manchester through funding the Critical Mass Project: Molecules, Clusters and Crystals (Grant references EP/IO14446/1 and EP/IO13563/1).

LIST OF SYMBOLS

A_0 Fixed needle cross sectional area (m^2)

a Dimensionless molecular latent heat of crystallisation

b Dimensionless thermodynamic parameter

C_e Equilibrium solution concentration (m^{-3})

C_0 Concentration of instantaneously nucleated crystallites (m^{-3})

C_s Concentration of sites on which clusters of the new phase can form (m^{-3})

ΔC_{max} Maximum concentration difference (m^{-3})

d Dimensionality of crystallite growth

d_0 Molecular diameter (m)

$\frac{dc_e}{dT}$ Rate of solubility change with temperature $(m^{-3}K^{-1})$

$f_{e,s}$ Molecular attachment frequency per growth site (s^{-1})

f_e^* Frequency of monomer attachment to the nucleus at $\Delta\mu = 0$ (s^{-1})

G Crystallite growth rate $(m\ s^{-1})$

H_0 Fixed disk or plate thickness (m)

i^* Number of molecules in critical nucleus

J Nucleation rate $(m^{-3}s^{-1})$

k Boltzmann constant (JK^{-1})

K_G Growth rate constant $\left(\mathrm{m}^{(\frac{1}{m})}s^{-1}\right)$

K_j Empirical parameter of nucleation rate $(m^{3(m_o-1)}s^{-1})$

K_J Nucleation rate constant $(m^{-3}s^{-1})$

k_n Nucleus numerical shape factor

k_v Crystallite growth shape factor (m^{3-d})

m_0 Nucleation rate order

m, n Crystallite growth exponents

N Number of crystallites

N_{det} Detectable number of crystallites

q Cooling rate $(K\ s^{-1})$

q_0 Parameter in the $u_c(q)$ dependence for both PN and IN $(K\ s^{-1})$

r^* Critical nucleus radius (m)

R Effective crystallite radius (m)

S Supersaturation ratio

T_0 Temperature at which crystallites are instantaneously nucleated (K)

T_c Crystallisation temperature (K)

T_e Solution saturation (or equilibrium) temperature (K)

ΔT Undercooling (K)

ΔT_c Critical undercooling for crystallisation (K)

u Relative undercooling

u_c Relative critical undercooling for crystallisation

u_0 Relative undercooling at the moment of crystallite IN

V Volume of solution (m^3)

V_c Total volume of crystallites (m^3)

V_n Volume of individual crystallite (m^3)

v_0 Volume of solute molecule in crystal (m^3)

α Fraction of crystallised volume α_{det} Detectable fraction of crystallised volume γ Interfacial tension of crystal nucleus in HON (Jm^{-2})

γ_{eff} Effective interfacial tension of crystal nucleus in $3D\ HEN$ (Jm^{-2})

λ Molecular latent heat of crystallisation (J)

Γ Complete gamma function

z Zeldovich factor

ψ Nucleation-activity factor

$\Delta\mu$ Supersaturation in terms of chemical potential difference (J)

LIST OF ABBREVIATIONS

DSC Differential scanning calorimetry

HEN Heterogeneous nucleation

HON Homogeneous nucleation

IN Instantaneous nucleation

$KBHR$ Kashchiev-Borissova-Hammond-Roberts approach

$KJMA$ Kolmogorov-Johnson-Mehl-Avrami approach

$MSZW$ Metastable zone width

PN Progressive nucleation

SD Standard deviation

$3D$ Three dimensional

REFERENCES

[1] D. Kashchiev, A. Borissova, R.B. Hammond, K.J. Roberts, Effect of cooling rate on the critical undercooling for crystallization, Journal of Crystal Growth, 312 (2010) 698-704.

[2] D. Kashchiev, A. Borissova, R.B. Hammond, K.J. Roberts, Dependence of the Critical Undercooling for Crystallization on the Cooling Rate, J Phys Chem B, 114 (2010) 5441-5446.

[3] G. Pahl, Biodiesel : growing a new energy economy, Chelsea Green Pub., White River Junction, Vt., 2005.

[4] K.-J. Kim, A. Mersmann, Estimation of Metastable Zone Width in different nucleation processes, Chemical Engineering Science, 56 (2001) 2315-2324.

[5] K. Sangwal, Novel approach to analyze Metastable Zone Width determined by the polythermal method: physical interpretation of various parameters, Crystal Growth and Design, 9 (2009) 942-950.

[6] J. Nyvlt, Kinetics of nucleation in solutions, Journal of Crystal Growth, 4 (1968) 377-383.

[7] J. Nyvlt, R. Rychly, J. Gottfried, J. Wurzelova, Metastable Zone Width of some aqueous solutions, Journal of Crystal Growth, 6 (1970) 151-162.

[8] N. Kubota, A new interpretation of metastable zone widths measured for unseeded solutions, Journal of Crystal Growth, 310 (2008) 629-634.

[9] K. Sangwal, A novel self-consistent Nyvlt-like equation for Metastable Zone Width determined by the polythermal method, Crystal Research and Technology, 44 (2009) 231-247.

[10] K. Sangwal, Recent developments in understanding of the metastable zone width of different solute-solvent systems, Journal of Crystal Growth, 318 (2001) 103-109.

[11] D. Kashchiev, Nucleation: basic theory with applications, Butterworth-Heinemann, Oxford, 2000.

[12] J.W. Mullin, Crystallization, 4th ed., Butterworth-Heinemann, Oxford, 2001.

[13] H. Gurbuz, O. B., Experimental determination of the Metastable Zone Width of borax decahydrate by ultrasonic velocity measurements, Journal of Crystal Growth, 252 (2003) 343-349.

[14] N. Lyczko., F. Espitalier, O. Louisnard, J. Schwartzentruber, Effect of ultrasound on the induction time and the metastable zone widths of potassium sulphate, Chem Eng J, 86 (2002) 233-241.

[15] O. Sahin, H. Dolas, H. Demir, Determination of nucleation kinetics of potassium tetraborate tetra hydrate Crystal, Research and Technology, 42 (2007) 766-772.

[16] P. Sayan, J. Ulrich, Effect of various impurities on the metastable zone width of Boric Acid, Crystal Research and Technology, 36 (2001) 411-417.

[17] D. Kashchiev, A. Firoozabadi, Kinetics of the initial stage of isothermal gas phase formation, J Chem Phys, 98 (1993) 4690-4699.

[18] D. Kashchiev, A. Firoozabadi, Induction time in crystallisation of gas hydrates, Journal of Crystal Growth, 250 (2003) 499-515.

[19] K. Sangwal, Additives and crystallization processes : from fundamentals to applications, Wiley, Chichester, 2007.

[20] C.H. MacGillavry, M. Wolthuis-Spuy, Crystal structure of an Orthorhombic modification of Methyl Stearate, Acta Crystalligraphica B26 (1970) 645-648.

[21] J.H. ter Horst, S. Jiang, Crystal nucleation rates from probability distributions of inductions times, Crystal Growth and Design, 11 (2011) 256-261.

[22] S. Teychené, B. Biscans, Nucleation kinetics of polymorphs: induction period and interfacial energy measurements, Crystal Growth and Design, 8 (2007) 1133-1139.

[23] R.A. Granberg, C. Ducreux, S. Gracin, A.C. Rasmuson, Primary nucleation of paracetamol in acetone-water mixtures, Chemical Engineering Science, 56 (2001) 2305-2313.

[24] F. Espitalier, B. Biscans, C. Laguérie, Particle design Part A: nucleation kinetics of ketoprofen, Chem Eng J, 68 (1997) 95-102.

[25] D. Turnbull, R.L. Cormia, Kinetics of crystal nucleation in some normal alkanes liquids, The Journal of Chemical Physics, 34 (1961) 820-831.

[26] K.J. Roberts, J.N. Sherwood, A. Stewart, The nucleation of n-eicosane crystals from solutions in n-dodecane in the presence of homologous impurities, Journal of Crystal Growth, 102 (1990) 419-426.

[27] A.R. Gerson, K.J. Roberts, J.N. Sherwood, An Instrument for the Examination of Nucleation from Solution and Its Application to the Study of Precipitation from Diesel Fuels and Solutions of Normal-Alkanes, Powder Technol, 65 (1991) 243-249.

[28] B.D. Chen, L.J. Brecevic, J. Garside, Nucleation of tetracosane in hydrocarbon solvents, 12th symposium on industrial crystallisation, 2 (1993) 4-059 - 054-064.

[29] D. Kashchiev, G.M. van Rosmalen, Review: nucleation in solutions revisited, Crystal Research and Technology, 38 (2003) 555-574.

[30] R.B. Hammond, K. Pencheva, K.J. Roberts, A structural-kinetic approach to model face-specific solution/crystal surface energy associated with the crystallization of acetyl salicylic acid from supersaturated aqueous/ethanol solution, Crystal Growth and Design, 6 (2006) 1324-1334.

[31] R.J. Davey, S.L.M. Schroeder, J.H. ter Horst, Nucleation of organic crystals-a molecular perspective, Angew Chem Int Edit, 52 (2013) 2166-2179.

[32] R.B. Hammond, C.Y. Ma, K.J. Roberts, P.Y. Ghi, R.K. Harris, Application of systematic search methods to studies of the structures of urea-dihydroxy benzene cocrystals, J Phys Chem B, 107 (2003) 11820-11826.

[33] R.B. Hammond, R.S. Hashim, C.Y. Ma, K.J. Roberts, Grid-based molecular modeling for pharmaceutical salt screening: Case example of 3,4,6,7,8,9-hexahydro-2H-pyrimido (1,2-a) pyrimidinium acetate, Journal of Pharmaceutical Sciences, 95 (2006) 2361-2372.

[34] R.B. Hammond, K. Pencheva, K.J. Roberts, Molecular modeling of crystal-crystal interactions between the alpha- and beta-polymorphic forms of L-glutamic acid using grid-based methods, Crystal Growth and Design, 7 (2007) 875-884.

[35] R.B. Hammond, K. Pencheva, K.J. Roberts, Structural variability within, and polymorphic stability of, nano-crystalline molecular clusters of L-glutamic acid and D-mannitol, modelled with respect to their size, shape and 'crystallisability', Crystengcomm, 14 (2012) 1069-1082.

[36] R.B. Hammond, S. Jeck, C.Y. Ma, K. Pencheva, K.J. Roberts, T. Auffret, An Examination of Binding Motifs Associated With Inter-Particle Interactions between Facetted Nano-Crystals of Acetylsalicylic Acid and Ascorbic Acid through the Application of Molecular Grid-Based Search Methods, Journal of Pharmaceutical Sciences, 98 (2009) 4589-4602.

[37] R.B. Hammond, K. Pencheva, K.J. Roberts, Simulation of energetic stability of facetted L-glutamic acid nanocrystalline clusters in relation to their polymorphic phase stability as a function of crystal size, J Phys Chem B, 109 (2005) 19550-19552.

[38] R.B. Hammond, K. Pencheva, K.J. Roberts, An examination of polymorphic stability and molecular conformational flexibility as a function of crystal size associated with the nucleation and growth of benzophenone, Faraday Discuss, 136 (2007) 91-106.

[39] R.B. Hammond, K. Pencheva, V. Ramachandran, K.J. Roberts, Application of grid-based molecular methods for modeling solvent-dependent crystal growth morphology: Aspirin crystallized from aqueous ethanolic solution, Crystal Growth and Design, 7 (2007) 1571-1574.

[40] R.B. Hammond, K. Pencheva, K.J. Roberts, T. Auffret, Quantifying solubility enhancement due to particle size reduction and crystal habit modification: Case study of acetyl salicylic acid, Journal of Pharmaceutical Sciences, 96 (2007) 1967-1973.

[41] G. Clydesdale, R.B. Hammond, V. Ramachandran, K.J. Roberts, Molecular modelling of the morphology of organic crystals in the presence of impurity species: Recent applications to naphthalene, phenanthrene, and caprolactam crystals, Mol Cryst Liq Cryst, 440 (2005) 235-257.

[42] G. Clydesdale, R.B. Hammond, K.J. Roberts, Molecular modeling of bulk impurity segregation and impurity-mediated crystal habit modification of naphthalene and phenanthrene in the presence of heteroimpurity species, J Phys Chem B, 107 (2003) 4826-4833.

[43] R.B. Hammond, V. Ramachandran, K.J. Roberts, Molecular modelling of the incorporation of habit modifying additives: alpha-glycine in the presence of L-alanine, Crystengcomm, 13 (2011) 4935-4944.

[44] P. Mougin, G. Clydesdale, R.B. Hammond, K.J. Roberts, Molecular and solid-state modeling of the crystal purity and morphology of epsilon-caprolactam in the presence of synthesis impurities and the imino-tautomeric species caprolactim, J Phys Chem B, 107 (2003) 13262-13272.

[45] N. Anuar, W.R.W. Daud, K.J. Roberts, S.K. Kamarudin, S.M. Tasirin, Morphology and Associated Surface Chemistry of L-Isoleucine Crystals Modeled under the Influence of L-Leucine Additive Molecules, Crystal Growth and Design, 12 (2012) 2195-2203.